EUROPEAN ORGANIZATION FOR NUCLEAR RESEARCH

CERN–SL–2002–016 (AP)
CLIC Note 511

Monte Carlo Generator for Muon Pair Production

H.Burkhardt[1], **S.R. Kelner**[2], **R.P. Kokoulin**[2]

[1] CERN, CH-1211 Geneva 23, Switzerland
[2] Moscow Engineering Physics Institute, Moscow 115409, Russia

Abstract

A Monte Carlo Generator for the electromagnetic pair production of muon pairs by high energy photons in matter is described. The computer code is designed as a standard electromagnetic process for GEANT4. The relevant formulas and algorithms are described and illustrated in detail.

Geneva, Switzerland

May 3, 2002

1 Introduction

High energy electrons, positrons and photons traversing matter loose quickly energy by bremsstrahlung ($\mathrm{e}^+, \mathrm{e}^-$ particles radiating a γ) and pair-production ($\gamma \rightarrow \mathrm{e}^+\mathrm{e}^-$). High energy $\mathrm{e}^+, \mathrm{e}^-$ particles in the pairs produced will again radiate photons which produce further pairs. This results in electromagnetic showers involving a cascade of many electrons and photons. The energy loss will typically reach a maximum within 5-10 radiation length (χ_0) and generally be contained within 20-30 radiation length (where $\chi_0 = 0.56\,\mathrm{cm}$ for lead and $\chi_0 = 0.35\,\mathrm{cm}$ for tungsten).

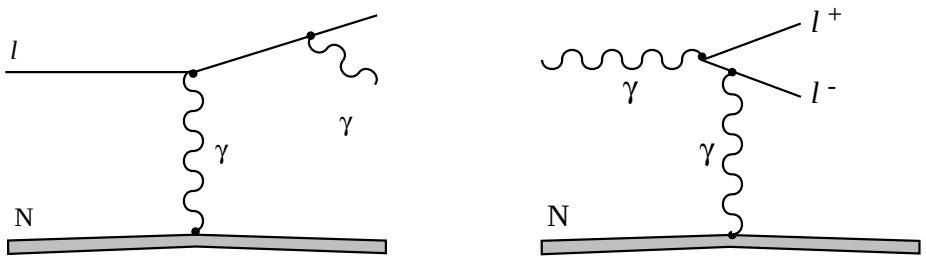

Figure 1: Diagrams for Bremsstrahlung (left) and lepton-pair production (right) in the presence of a nucleus N.

The diagrams for the two processes discussed are shown in Fig. 1. They are not restricted to electrons and apply more generally to the interaction between photons and charged leptons (e, μ, τ). The cross sections are of the order of $4Z^2\alpha r_c^2$, where Z is the charge of the nucleus, the electromagnetic coupling constant $\alpha \approx 1/137$ and $r_c = e^2/(4\pi\epsilon_0 mc^2)$ the classical radius of the charged particle involved. Compared to electron-pair production, the muon-pair production is suppressed by the square of the mass ratio, with $(m_e/m_\mu)^2 = 2.34 \times 10^{-5}$. Once produced however, the muons do also loose their energy much slower and become the dominant component as far as leakage from thick targets is concerned.

Monte Carlo simulation packages for electromagnetic showers like EGS [1, 2] and GEANT [3] have been available for many years and are widely used. The pair production in these programs is restricted to electrons. This is adequate for predictions of the energy loss in calorimeters, but not for leakage through shielding and collimators.

Estimates for muon background from linear colliders relied on dedicated programs [4] based on cross sections from Tsai [5, 6] or a combination of dedicated muon-pair production and follow up of the muons by GEANT3 [7].

First estimates for CLIC indicate background rates of about 1 muon in the detector for 10^5 electrons hitting a collimator [8]. Assuming a fraction of 10^{-3} tail particles to collimate and nominal bunch intensities, this could result into thousands of muons per bunch train in the detector. A good simulation of muon production and energy loss is therefore rather essential both for the CLIC beam delivery and detector design.

This report describes the algorithms for the dominant process of muon production in electromagnetic showers, which is γ conversion into a muon-pair. The algorithms are based on the work of Kelner, Kokoulin and Petrukhin [9–11] and closely related to Bremsstrahlung from muons. A more complete survey of processes leading to muons and in particular the implementation of positron annihilation with atomic electrons into muons $\mathrm{e}^+\mathrm{e}^- \rightarrow \mu^+\mu^-$ in Geant4 is planned. With the integration into GEANT4, secondary muon production in the cascade and the simulation of the energy loss of the muons in matter are also taken into account. There is a world wide collaboration on GEANT4 [12] with up-to-date code and documentation available from the web [13].

2 Cross section and energy sharing

We consider pair production of muons in the field of the nucleus. Pair production on atomic electrons $\gamma + e \to e + \mu^+ + \mu^-$ has a threshold of $2m_\mu(m_\mu + m_e)/m_e \approx 43.9$ GeV and a much lower cross section than the process on the nucleus up to several hundred GeV. At higher energies, the cross section on atomic electrons represents a correction of $\sim 1/Z$ to the total cross section.

For the approximately elastic scattering considered here, there is only momentum but no energy transferred to the nucleon. The photon energy is fully shared by the two muons according to

$$E_\gamma = E_\mu^+ + E_\mu^- \tag{1}$$

or in terms of energy fractions

$$x_+ = \frac{E_\mu^+}{E_\gamma} \qquad x_- = \frac{E_\mu^-}{E_\gamma} \qquad x_+ + x_- = 1 \; .$$

The differential cross section for electromagnetic pair creation of muons in terms of the energy fractions of the muons is

$$\frac{d\sigma}{dx_+} = 4\,\alpha\,Z^2\,r_c^2\left(1 - \frac{4}{3}\,x_+x_-\right)\log(W) \; , \tag{2}$$

where Z is the charge of the nucleus, r_c the classical radius of the particles which are pair produced (here muons) and

$$W = W_\infty\,\frac{1 + (D_n\sqrt{e} - 2)\,\delta\,/m_\mu}{1 + B\,Z^{-1/3}\,\sqrt{e}\,\delta\,/m_e} \tag{3}$$

where

$$W_\infty = \frac{B\,Z^{-1/3}}{D_n}\,\frac{m_\mu}{m_e} \qquad \delta = \frac{m_\mu^2}{2\,E_\gamma\,x_+x_-} \qquad \sqrt{e} = 1.6487\ldots$$

and

$$\begin{array}{rrll} B = 202.4 & D_n = & 1.49 & \text{for Hydrogen and} \\ B = 183 & D_n = & 1.54\,A^{0.27} & \text{otherwise.} \end{array} \tag{4}$$

These formulas are obtained from the differential cross section for muon bremsstrahlung [10] by means of crossing relations. The formulas take the screening of the field of the nucleus by the atomic electrons in the Thomas-Fermi model into account, and also the finite size of the nucleus which is essential for the problem under consideration. The formulas give good results for $E_\gamma \gg m_\mu$. The fact that they are approximate close to threshold is of little practical importance. Close to threshold, the cross section is small and the few low energy muons produced will not travel too far. The cross section calculated from Eq. (2) is positive for $E_\gamma > 4m_\mu$ and

$$x_{\min} \le x \le x_{\max} \quad \text{with} \quad x_{\min} = \frac{1}{2} - \sqrt{\frac{1}{4} - \frac{m_\mu}{E_\gamma}} \qquad x_{\max} = \frac{1}{2} + \sqrt{\frac{1}{4} - \frac{m_\mu}{E_\gamma}} \; , \tag{5}$$

except for very asymmetric pair-production, close to threshold, which can easily be taken care of by setting explicitly $\sigma = 0$ whenever $\sigma < 0$.

Note that the differential cross section is symmetric in x_+, x_- and that

$$x_+x_- = x - x^2$$

where x stands for both x_+ and x_-. Defining a constant

$$\sigma_0 = 4\,\alpha\,Z^2\,r_c^2\log(W_\infty)\ . \tag{6}$$

we can rewrite the differential cross section Eq. (2) normalized and symmetric as function of x as

$$\frac{1}{\sigma_0}\,\frac{d\sigma}{dx} = \left[1 - \frac{4}{3}\,(x - x^2)\right]\,\frac{\log W}{\log W_\infty}\ . \tag{7}$$

This is shown in Fig. 2 for several elements and a wide range of photon energies. The asymptotic differential cross section for $E_\gamma \to \infty$

$$\frac{1}{\sigma_0}\,\frac{d\sigma_\infty}{dx} = 1 - \frac{4}{3}\,(x - x^2)$$

is also shown.

3 Parametrization of the total cross section

The total cross section is obtained by integration of the differential cross section Eq. (2), that is

$$\sigma_{\rm tot}(E_\gamma) = \int_{x_{\rm min}}^{x_{\rm max}} \frac{d\sigma}{dx_+}\,dx_+ = 4\,\alpha\,Z^2\,r_c^2\int_{x_{\rm min}}^{x_{\rm max}}\left(1 - \frac{4}{3}\,x_+x_-\right)\log(W)\,dx_+\ . \tag{8}$$

W is a function of x_+, E_γ and Z, A of the element, see Eq. (3). Table 1 gives numerical values.

Table 1: Numerical values of W fo $x_+ = 0.5$ for different elements.

E_γ GeV	W for H	W for Be	W for Cu	W for Pb
1	2.11	1.594	1.3505	5.212
10	19.4	10.85	6.803	43.53
100	191.5	102.3	60.10	332.7
1000	1803	919.3	493.3	1476.1
10000	11427	4671	1824	1028.1
∞	28087	8549	2607	1339.8

Values of the total cross section obtained by numerical integration are listed in Table 2 for 4 different elements. Units are μbarn, where $1\,\mu{\rm barn} = 10^{-34}\,{\rm m}^2$.

Table 2: Numerical values for the total cross section

E_γ GeV	$\sigma_{\rm tot}$, H μbarn	$\sigma_{\rm tot}$, Be μbarn	$\sigma_{\rm tot}$, Cu μbarn	$\sigma_{\rm tot}$, Pb μbarn
1	0.01559	0.1515	5.047	30.22
10	0.09720	1.209	49.56	334.6
100	0.1921	2.660	121.7	886.4
1000	0.2873	4.155	197.6	1476
10000	0.3715	5.392	253.7	1880
∞	0.4319	6.108	279.0	2042

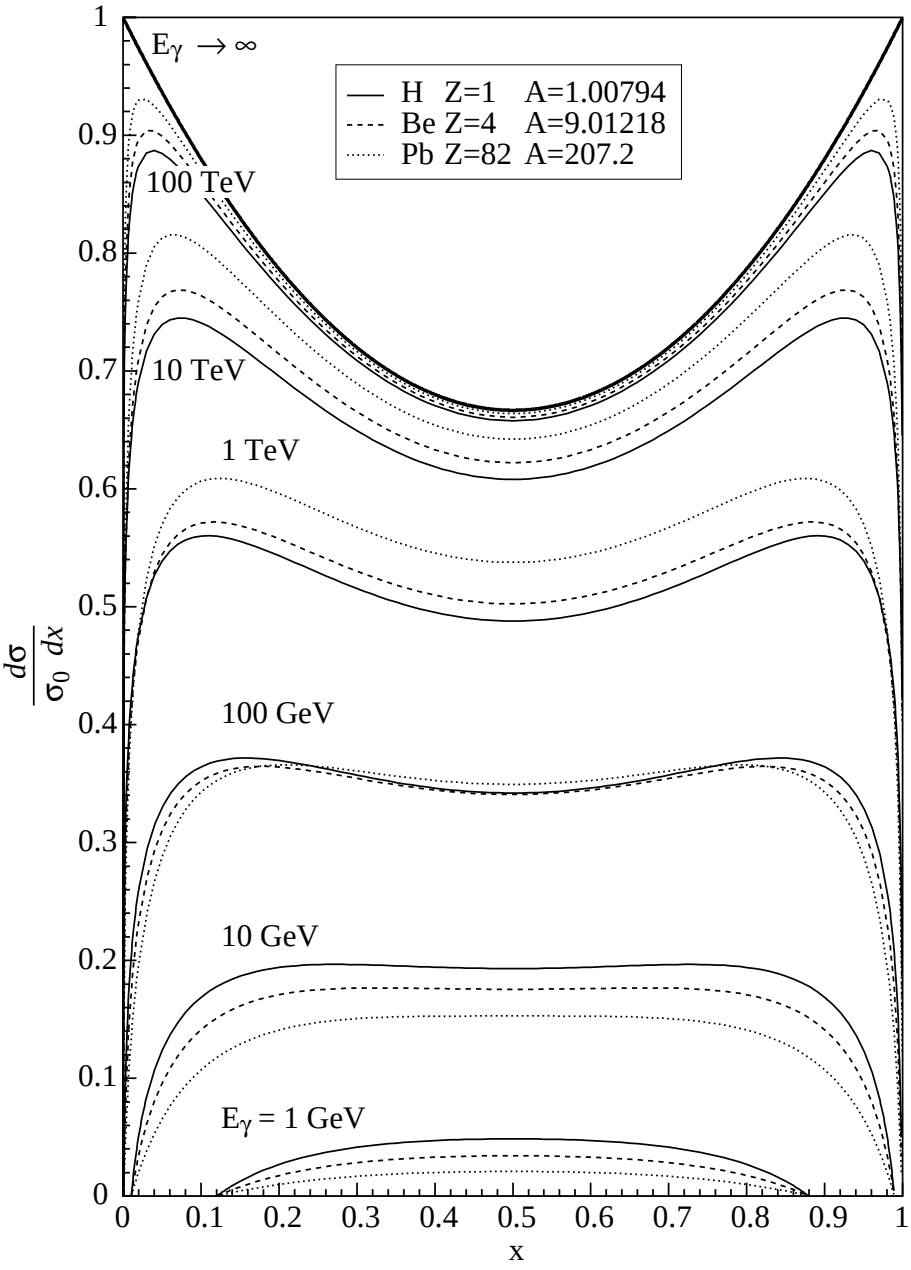

Figure 2: Normalized differential cross section for pair production as function of x, the energy fraction of the photon energy carried by one of the leptons in the pair. The function is shown for 3 different elements, Hydrogen, Beryllium and Lead and for a wide range of photon energies.

Well above threshold, the total cross section rises about linearly in $\log(E_\gamma)$ with the slope

$$W_M = \frac{1}{4\,D_n\,\sqrt{e}\,m_\mu} \tag{9}$$

until it saturates by screening at σ_∞, see Fig. 3, where

$$\sigma_\infty = \frac{7}{9}\,\sigma_0 \qquad \text{and} \qquad \sigma_0 = 4\,\alpha\,Z^2\,r_c^2\,\log(W_\infty)\ . \tag{10}$$

Table 3 gives numerical values of W_M.
The total cross section is parametrized as

$$\sigma_{\rm par} = \frac{28\,\alpha\,Z^2\,r_c^2}{9}\ \log(1 + W_M C_f E_g)\ . \tag{11}$$

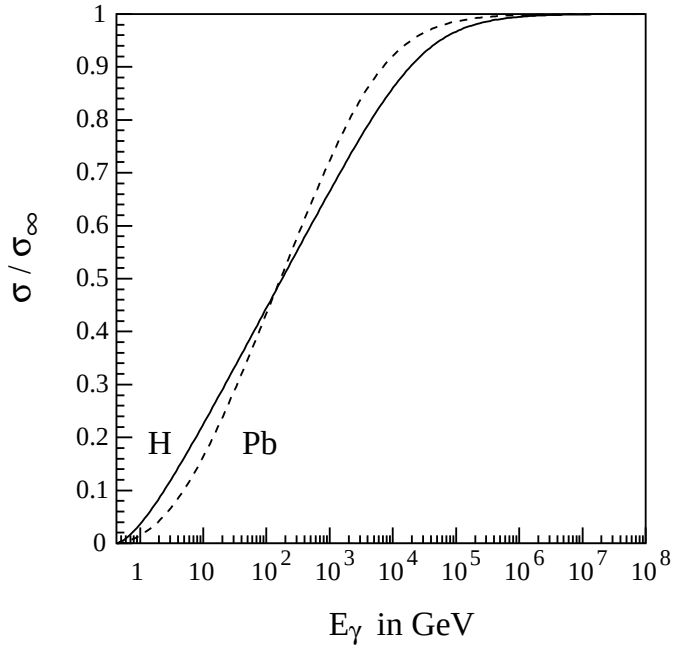

Figure 3: Total cross section for the Bethe Heitler process $\gamma \rightarrow \mu^+\mu^-$ as function of the photon energy E_γ in Hydrogen and Lead, normalized to the asymptotic cross section σ_∞.

Table 3: Numerical values of W_M.

Element	W_M 1/GeV
H	0.963169
Be	0.514712
Cu	0.303763
Pb	0.220771

The threshold behaviour in the cross section was found to be well approximated by the power $t = 1.479 + 0.00799\, D_n$ and the saturation with power $s = -0.88$, both included in

$$E_g = \left(1 - \frac{4m_\mu}{E_\gamma}\right)^t \left(W_{\rm sat}^s + E_\gamma^s\right)^{1/s} \ , \tag{12}$$

where

$$W_{\rm sat} = \frac{W_\infty}{W_M} = B\, Z^{-1/3}\, \frac{4\,\sqrt{e}\, m_\mu^2}{m_e} \ .$$

The agreement at lower energies is improved using an empirical correction factor, applied to the slope W_M of the form

$$C_f = \left[1 + 0.04 \log\left(1 + \frac{E_c}{E_\gamma}\right)\right] \ ,$$

where

$$E_c = \left[-18. + \frac{4347.}{B\, Z^{-1/3}}\right] \ \text{GeV} \ .$$

Comparison with the numerical integration of the exact cross section shows, that the accuracy of the parametrization is better than 2%, see Fig. 4.

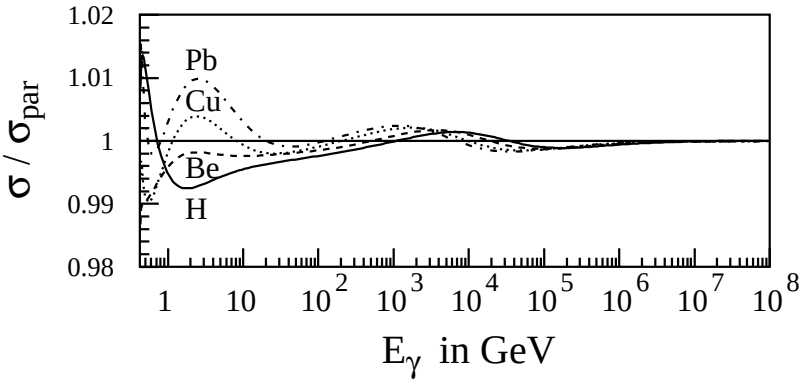

Figure 4: Ratio of numerically integrated and parametrized total cross sections as function of E_γ for Hydrogen, Beryllium, Copper and Lead.

4 Multi-differential cross section and angular variables

The angular distributions are based on the multi-differential cross section for lepton pair production in the field of the Coulomb centre

$$\frac{d\sigma}{dx_+\,du_+\,du_-\,d\varphi} = \frac{4\,Z^2\alpha^3}{\pi}\,\frac{m_\mu^2}{q^4}\,u_+\,u_- \left\{\frac{u_+^2+u_-^2}{(1+u_+^2)\,(1+u_-^2)} - 2x_+x_-\left[\frac{u_+^2}{(1+u_+^2)^2}+\frac{u_-^2}{(1+u_-^2)^2}\right] - \frac{2u_+u_-(1-2x_+x_-)\,\cos\varphi}{(1+u_+^2)\,(1+u_-^2)}\right\}\,. \tag{13}$$

Here

$$u_\pm = \gamma_\pm\theta_\pm \quad , \qquad \gamma_\pm = \frac{E_\mu^\pm}{m_\mu} \quad , \qquad q^2 = q_\parallel^2 + q_\perp^2 \quad , \tag{14}$$

where

$$q_\parallel^2 = q_{\min}^2\,(1+x_-u_+^2+x_+u_-^2)^2\,, \quad q_\perp^2 = m_\mu^2\left[(u_+-u_-)^2+2\,u_+u_-(1-\cos\varphi)\right]\,. \tag{15}$$

q^2 is the square of the momentum $\mathbf{q}$ transferred to the target and $q_\parallel^2$, $q_\perp^2$ the squares of the components of the vector $\mathbf{q}$, which are parallel and perpendicular to the initial photon momentum, respectively. The minimum momentum transfer is $q_{\min} = m_\mu^2/(2E_\gamma\,x_+x_-)$.
The muon vectors have the components

$$\begin{aligned} \mathbf{p}_+ &= p_+\,(\ \sin\theta_+\cos(\varphi_0+\varphi/2)\,,\quad \sin\theta_+\sin(\varphi_0+\varphi/2)\,,\,\cos\theta_+)\,, \\ \mathbf{p}_- &= p_-\,(-\sin\theta_-\cos(\varphi_0-\varphi/2)\,,\,-\sin\theta_-\sin(\varphi_0-\varphi/2)\,,\,\cos\theta_-)\,, \end{aligned} \tag{16}$$

where $p_\pm = \sqrt{E_\pm^2-m_\mu^2}$. The initial photon direction is taken as the z-axis. The cross section Eq. (13) does not depend on φ_0. Since we have azimuthal symmetry, φ_0 can simply be sampled at random in the interval $(0,\,2\,\pi)$.

Eq. (13) is too complicated for efficient Monte Carlo generation. To simplify, the cross section is rewritten in a u_+, u_- symmetric way using a new variable u and small parameters ξ, β, where $u_\pm = u \pm \xi/2$ and $\beta = u\,\varphi$. When higher powers in small parameters are dropped, the differential

cross section in terms of u, ξ, β becomes

$$\frac{d\sigma}{dx_+\, d\xi\, d\beta\, u du} = \frac{4\, Z^2\alpha^3}{\pi} \frac{m_\mu^2}{\left(q_\parallel^2 + m_\mu^2(\xi^2+\beta^2)\right)^2} \left\{ \xi^2 \left[\frac{1}{(1+u^2)^2} - 2\, x_+ x_- \frac{(1-u^2)^2}{(1+u^2)^4} \right] + \frac{\beta^2(1-2x_+x_-)}{(1+u^2)^2} \right\}, \tag{17}$$

where, in this approximation,

$$q_\parallel^2 = q_{\min}^2\, (1+u^2)^2\, .$$

For Monte Carlo generation, it will be convenient to replace ξ, β by polar coordinates ρ, ψ with $\xi = \rho\, \cos\psi$ and $\beta = \rho\, \sin\psi$. From integration over ψ and using symbolically du^2 where $du^2 = 2u\, du$, we have

$$\frac{d\sigma}{dx_+\, d\rho\, du^2} = \frac{4Z^2\alpha^3}{m_\mu^2} \frac{\rho^3}{(q_\parallel^2/m_\mu^2 + \rho^2)^2} \left\{ \frac{1-x_+x_-}{(1+u^2)^2} - \frac{x_+x_-(1-u^2)^2}{(1+u^2)^4} \right\}. \tag{18}$$

Integration with logarithmic accuracy over ρ gives

$$\int \frac{\rho^3\, d\rho}{(q_\parallel^2/m_\mu^2 + \rho^2)^2} \approx \int\limits_{q_\parallel/m_\mu}^{1} \frac{d\rho}{\rho} = \log\left(\frac{m_\mu}{q_\parallel}\right). \tag{19}$$

Within the logarithmic accuracy, one can replace $\log(m_\mu/q_\parallel)$ by $\log(m_\mu/q_{\min})$, so that

$$\frac{d\sigma}{dx_+\, du^2} = \frac{4\, Z^2\alpha^3}{m_\mu^2} \left\{ \frac{1-x_+x_-}{(1+u^2)^2} - \frac{x_+x_-(1-u^2)^2}{(1+u^2)^4} \right\} \log\left(\frac{m_\mu}{q_{\min}}\right). \tag{20}$$

With the substitution $u^2 = 1/t - 1$, $du^2 = -dt\, /t^2$ we get

$$\frac{d\sigma}{dx_+\, dt} = \frac{4\, Z^2\alpha^3}{m_\mu^2} \left[1 - 2\, x_+x_- + 4\, x_+x_- t\, (1-t)\right] \log\left(\frac{m_\mu}{q_{\min}}\right). \tag{21}$$

Atomic screening and the finite nuclear radius may be taken into account by multiplying the differential cross section determined by Eq. (17) with the factor (please note that after integration over ρ, the q-dependence is lost)

$$\left(F_a(q) - F_n(q)\right)^2, \tag{22}$$

where F_a and F_n are atomic and nucleus form factors.

5 Steps in the Monte Carlo generation of $\gamma \longrightarrow \mu^+\mu^-$

Given is the photon energy E_γ and Z, A of the material in which the γ converts. The probability for the conversions to take place is calculated according to the parametrized total cross section Eq. (11). The next step is to determine how the photon energy is shared between the μ^+ and μ^-, that is to generate x_+ according to Eq. (2). The directions of the muons are then generated via auxiliary variables $t,\ \rho,\ \psi$.

Now a detailed description of the algorithms employed in every step. $R_{1,2,3,4,\ldots}$ are random numbers with a flat distribution in the interval (0,1). The generation proceeds as follows.

1) Sampling of the positive muon energy $E_\mu^+ = x_+ E_\gamma$.
This is done using the rejection technique. x_+ is first sampled flat within kinematic limits using

$$x_+ = x_{\min} + R_1(x_{\max} - x_{\min})$$

and then brought to the shape of Eq. (2) by keeping all x_+ which satisfy

$$\left(1 - \frac{4}{3}\,x_+x_-\right)\frac{\log(W)}{\log(W_{\max})} < R_2\,,$$

where $W_{\max} = W(x_+ = 1/2)$ is the maximum value of W, obtained for symmetric pair-production at $x_+ = 1/2$. About 60% of the events are kept in this step. Results of a Monte Carlo generation of x_+ are illustrated in Fig. 5. The shape of the histograms agrees with the differential cross section illustrated in Fig. 2.

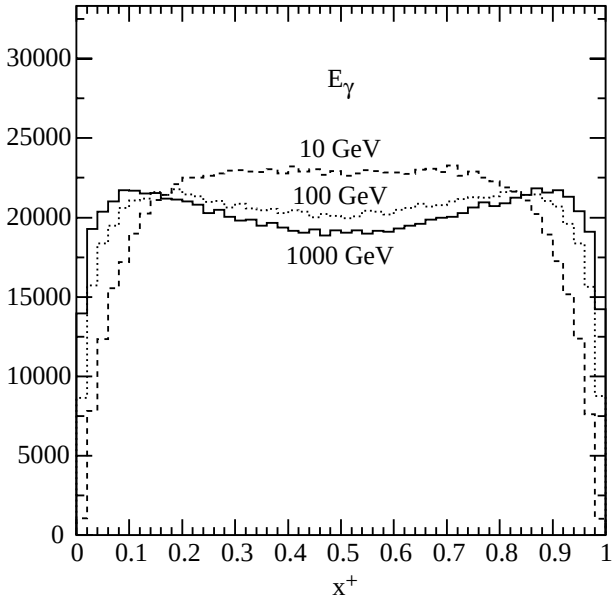

Figure 5: Histogram of generated x_+ distributions for Beryllium at three different photon energies. The total number of entries at each energy is 10^6.

2) Generate t.
The distribution in t is obtained from Eq.(21) as

$$f_1(t)\,dt = \frac{1 - 2\,x_+x_- + 4\,x_+x_-t\,(1-t)}{1 + C_1/t^2}\,dt\,, \quad 0 < t \le 1\,. \tag{23}$$

with form factors taken into account by

$$C_1 = \frac{(0.35\,A^{0.27})^2}{x_+x_-\,E_\gamma/m_\mu}\,. \tag{24}$$

In the interval considered, the function $f_1(t)$ will always remain below

$$\max[f_1(t)] = \frac{1 - x_+x_-}{1 + C_1}\,.$$

For small x_+ and high E_γ, $f_1(t)$ approaches a value of 1, see Fig. 6.

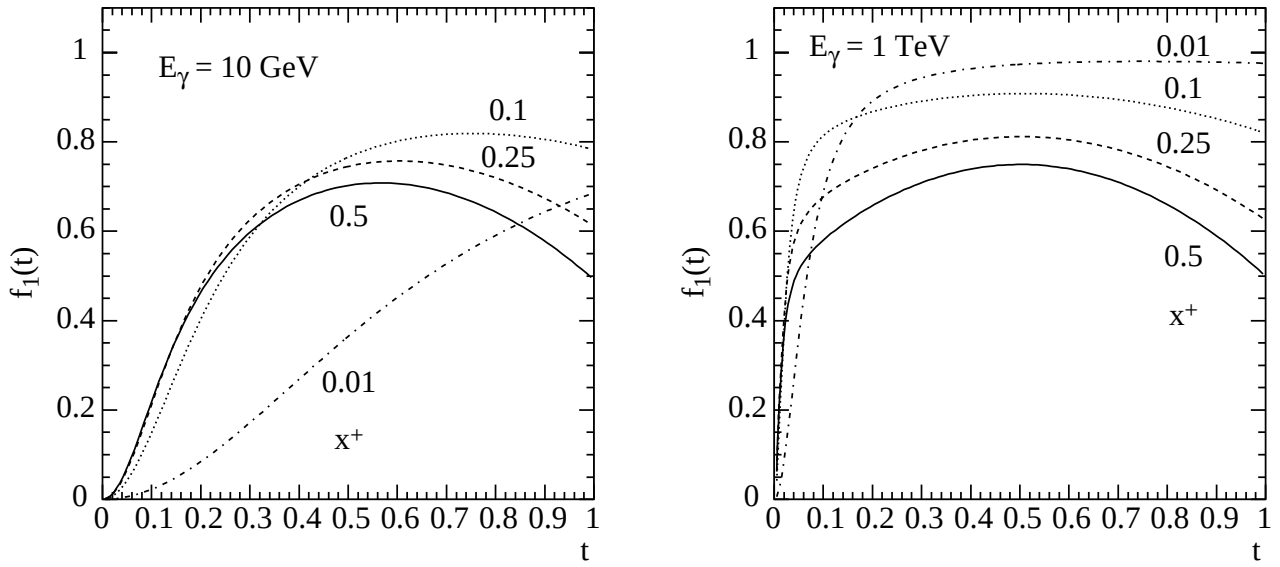

Figure 6: The function $f_1(t)$ at $E_\gamma = 10\,\mathrm{GeV}$ (left) and $E_\gamma = 1\,\mathrm{TeV}$ (right) in Beryllium for different values of x_+.

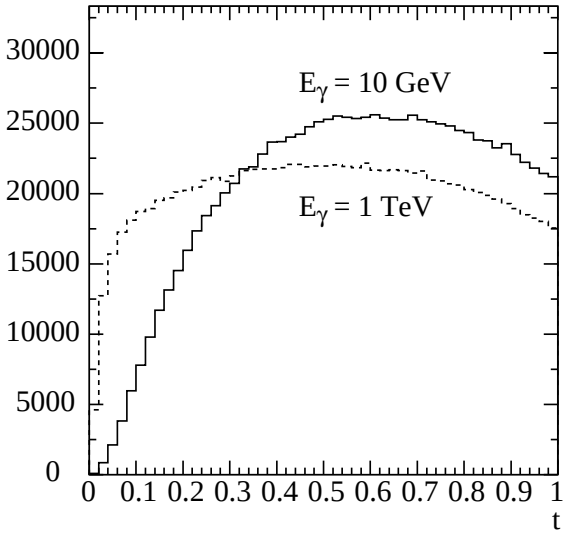

Figure 7: Histogram of generated t distributions for $E_\gamma = 10\,\mathrm{GeV}$ (solid line) and $E_\gamma = 100\,\mathrm{GeV}$ (dashed line) with 10^6 events each.

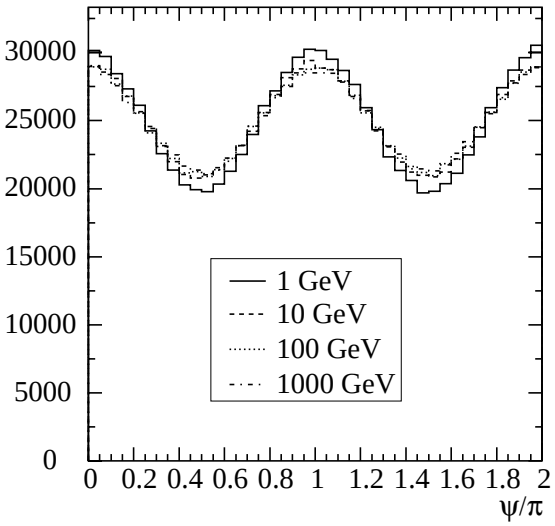

Figure 8: Histograms of generated ψ distributions for Beryllium at four different photon energies.

The Monte Carlo generation is done using the rejection technique. About 70% of the generated numbers are kept in this step. Generated t-distributions are shown in Fig. 7.

3) Generate ψ by the rejection technique using t generated in the previous step for the frequency distribution

$$f_2(\psi) = \Big[1 - 2\,x_+x_- + 4\,x_+x_-t\,(1-t)\,(1+\cos(2\psi))\Big]\,, \qquad 0 \le \psi \le 2\pi\,. \tag{25}$$

The maximum of $f_2(\psi)$ is

$$\max[f_2(\psi)] = 1 - 2\,x_+x_-\,[1 - 4\,t\,(1-t)]\,. \tag{26}$$

Generated distributions in ψ are shown in Fig. 8.

4) Generate ρ.
The distribution in ρ has the form

$$f_3(\rho)\, d\rho = \frac{\rho^3\, d\rho}{\rho^4 + C_2}\,, \quad 0 \le \rho \le \rho_{\max}\,, \tag{27}$$

where

$$\rho^2_{\max} = \frac{1.9}{A^{0.27}} \left(\frac{1}{t} - 1\right)\,, \tag{28}$$

and

$$C_2 = \frac{4}{\sqrt{x_+ x_-}} \left[\left(\frac{m_\mu}{2E_\gamma x_+ x_-\, t}\right)^2 + \left(\frac{m_e}{183\, Z^{-1/3}\, m_\mu}\right)^2\right]^2\,. \tag{29}$$

The ρ distribution is obtained by direct transformation applied to uniform random numbers R_i according to

$$\rho = \left[C_2(\exp(\beta\, R_i) - 1)\right]^{1/4}\,, \tag{30}$$

where

$$\beta = \log\left(\frac{C_2 + \rho^4_{\max}}{C_2}\right)\,. \tag{31}$$

Generated distributions of ρ are shown in Fig. 9

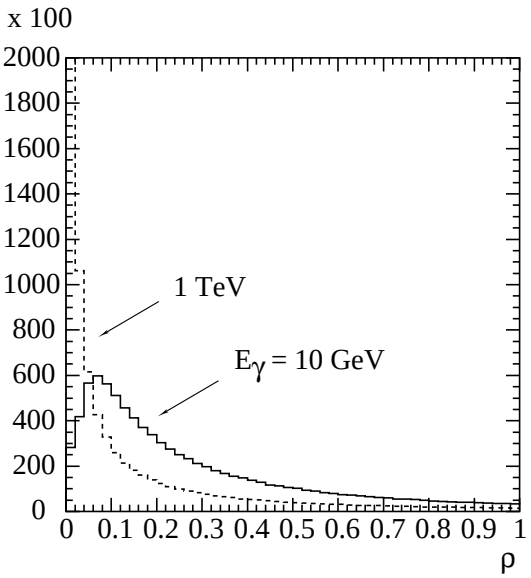

Figure 9: Histograms of generated ρ distributions for Beryllium at two different photon energies. The total number of entries at each energy is 10^6.

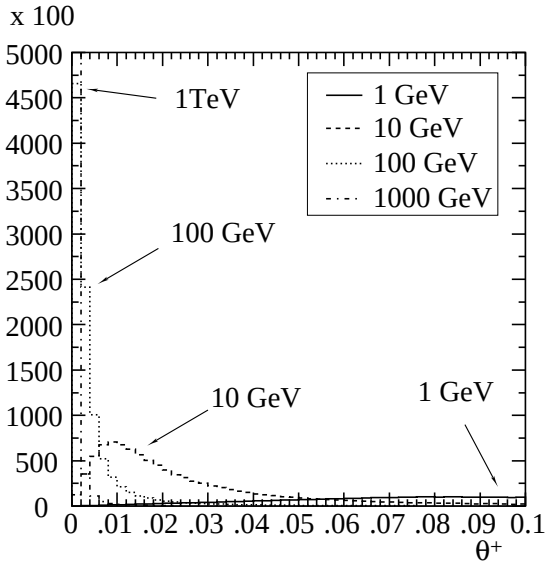

Figure 10: Histogram of generated θ_+ distributions at different photon energies.

5) Calculate θ_+, θ_- and φ from t, ρ, ψ with

$$\gamma_\pm = \frac{E^\pm_\mu}{m_\mu} \qquad \text{and} \qquad u = \sqrt{\frac{1}{t} - 1}\,. \tag{32}$$

according to

$$\theta_+ = \frac{1}{\gamma_+}\left(u + \frac{\rho}{2}\cos\psi\right), \quad \theta_- = \frac{1}{\gamma_-}\left(u - \frac{\rho}{2}\cos\psi\right) \quad \text{and} \quad \varphi = \frac{\rho}{u}\sin\psi\,. \tag{33}$$

The muon vectors can now be constructed from Eq. (16), where φ_0 is chosen randomly between 0 and 2π. Fig. 10 shows distributions of θ_+ at different photon energies (in Beryllium). The spectra peak around $1/\gamma$ as expected.

The most probable values are $\theta_+ \sim m_\mu/E_\mu^+ = 1/\gamma_+$. In the small angle approximation used here, the values of θ_+ and θ_- can in principle be any positive value from 0 to ∞. This may lead in the simulation (with a very small probability, of the order of m_μ/E_γ) to un-physical events in which θ_+ or θ_- is greater than π. To avoid this, a limiting angle $\theta_{\rm cut} = \pi$ is introduced, and the angular sampling repeated, whenever $\max(\theta_+, \theta_-) > \theta_{\rm cut}$.

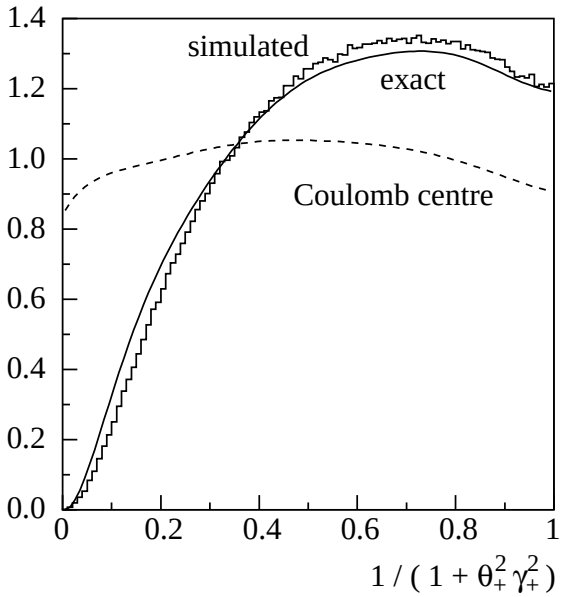

Figure 11: Angular distribution of positive (or negative) muons. The solid curve represents the results of the exact calculations. The histogram is the simulated distribution. The angular distribution for pairs created in the field of the Coulomb centre (point-like target) is shown as dashed curve for comparison.

Figs. 11,12 and 13 show distributions of the simulated angular characteristics of muon pairs in comparison with results of exact calculations. The latter were obtained by means of numerical integration of the squared matrix elements with respective nucleus and atomic form factors. All these calculations were made for iron, $E_\gamma = 10\,\mathrm{GeV}$ and $x_+ = 0.3$. As it is seen from Fig. 11, wide angle pairs (at low values of the argument in the figure) are suppressed in comparison with the Coulomb centre approximation, which is explained by the influence of the finite nuclear size (comparable to the inverse mass of the muon). Typical angles of particle emission are of the order of $1/\gamma_\pm = m_\mu/E_\mu^\pm$ (Fig. 12). Fig. 13 illustrates the influence of the momentum transferred to the target on the angular characteristics of the produced pair; in the frame of the often used model which neglects target recoil, the pair particles would be symmetric in transverse momenta (and coplanar with the initial photon).

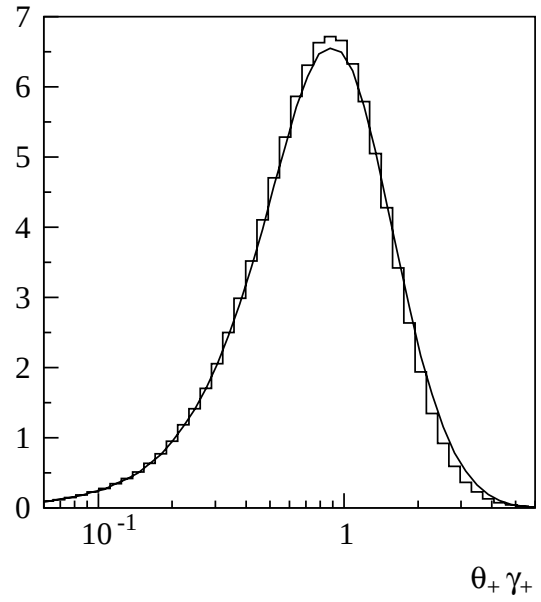

Figure 12: Angular distribution in logarithmic scale. The curve corresponds to the exact calculations and the histogram is the simulated distribution.

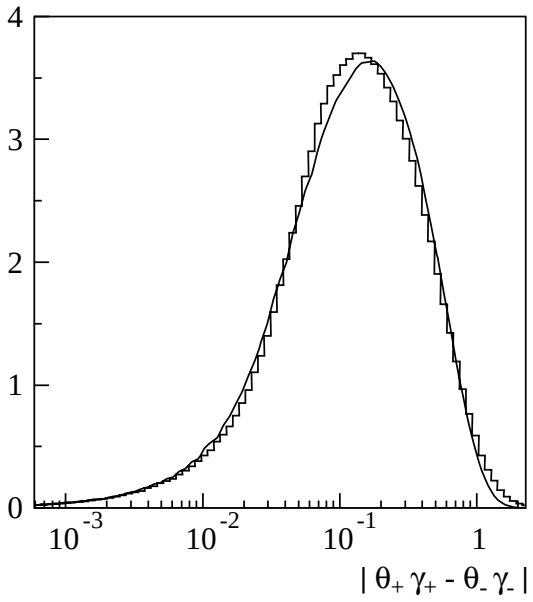

Figure 13: Distribution in the difference of transverse momenta of positive and negative muons (with logarithmic x-scale).

Acknowledgments

We would like to thank M. Maire for his help and advice on standard electromagnetic processes in Geant4 and G. Folger for help on the computer environment setup.

The code described here has been committed to the GEANT4 repository as standard electromagnetic process “GammaToMuPair” and will be generally available from the web [13] in future GEANT4 releases (the next is scheduled for June 2002).

References

[1] R. L. Ford and W. R. Nelson, “The EGS code system: Computer programs for the Monte Carlo Simulation of Electromagnetic Cascade Showers (Version 3),”. SLAC-0210.

[2] W. R. Nelson, H. Hirayama, and D. W. O. Rogers, “The EGS4 code system,”. SLAC-0265.

[3] R. Brun, R. Hagelberg, M. Hansroul, and J. C. Lassalle, “GEANT: Simulation program for Particle Physics Experiments. User Guide and Reference Manual,”. CERN-DD-78-2-REV.

[4] S. H. Rokni, L. P. Keller, and W. R. Nelson, “Calculation of muon background in electron accelerators using the Monte Carlo computer program MUCARLO,”. SLAC-PUB-7054, (1996).

[5] Y.-S. Tsai, “Pair production and Bremsstrahlung of charged leptons,” *Rev. Mod. Phys.* **46** (1974) 815–851.

[6] Y.-S. Tsai, “Pair production and Bremsstrahlung of charged leptons (erratum),” *Rev. Mod. Phys.* **49** (1977) 421–423.

[7] **TESLA** Collaboration, M. Sachwitz and H. J. Schreiber, "Muon background in a 500-GeV TESLA linear collider,". TESLA-94-27.

[8] R. Assmann, H. Burkhardt, S. Fartoukh, J.-B. Jeanneret, J. Pancin, S. Redaelli, T. Risselada, F. Zimmermann, and H. Schreiber, "Overview of the CLIC collimation design,". Prepared for IEEE Particle Accelerator Conference (PAC 2001), Chicago, Illinois, 18-22 Jun 2001.

[9] A. Petrukhin and V. Shestakov, "The influence of the nuclear and atomic form factors on the muon bremsstrahlung cross section,". Proc. 10th Intern. Cosmic Ray Conf., Calgary, 1967, Canad.J.Phys. 46, S377, 1968.

[10] S. R. Kelner, R. P. Kokoulin, and A. A. Petrukhin, "About cross-section for high-energy muon bremsstrahlung,". Moscow Phys. Eng. Inst. 024-95, 1995. 31pp.

[11] S. Kelner, "Angular distribution of muons in $\gamma \to \mu^+\mu^-$ conversion." Notes of January to April 2002 (unpublished).

[12] S. Giani, S. Ravndal, and M. Maire, "GEANT4: a world-wide collaboration to build object oriented HEP simulation software,". Talk given at Computing in High-energy Physics (CHEP 97), Berlin, Germany, 7-11 Apr 1997.

[13] Geant4 home page http://wwwinfo.cern.ch/asd/geant4/geant4.html, Physics reference manual http://wwwinfo.cern.ch/asd/geant4/G4UsersDocuments/UsersGuides/PhysicsReferenceManual/html .